Received: 20 September 2024 | Accepted: 13 February 2025

DOI: 10.1002/hem3.70120

HemaSphere eha

ARTICLE

Orchestration of human multi-lineage hematopoietic cell development by humanized in vivo bone marrow models

Laurent Renou[1,2,3] | Wenjie Sun[4,^] | Chloe Friedrich[5,^] | Klaudia Galant[1,2,3] | Cecile Conrad[4] | Anne Consalus[1,2,3] | Evelia Plantier[1,2,3] | Katharina Schallmoser[6] | Linda Krisch[6] | Vilma Barroca[1,3,7] | Saryami Devanand[1,3,7] | Nathalie Dechamps[1,3,8] | Andreas Reinisch[9,10] | Jelena Martinovic[11] | Alessandra Magnani[12] | Lionel Faivre[13] | Daniel Lewandowski[1,2,3] | Julien Calvo[1,2,3] | Leila Perie[4,^] | Olivier Kosmider[2,5,^] | Françoise Pflumio[1,2,3]

Graphical Abstract

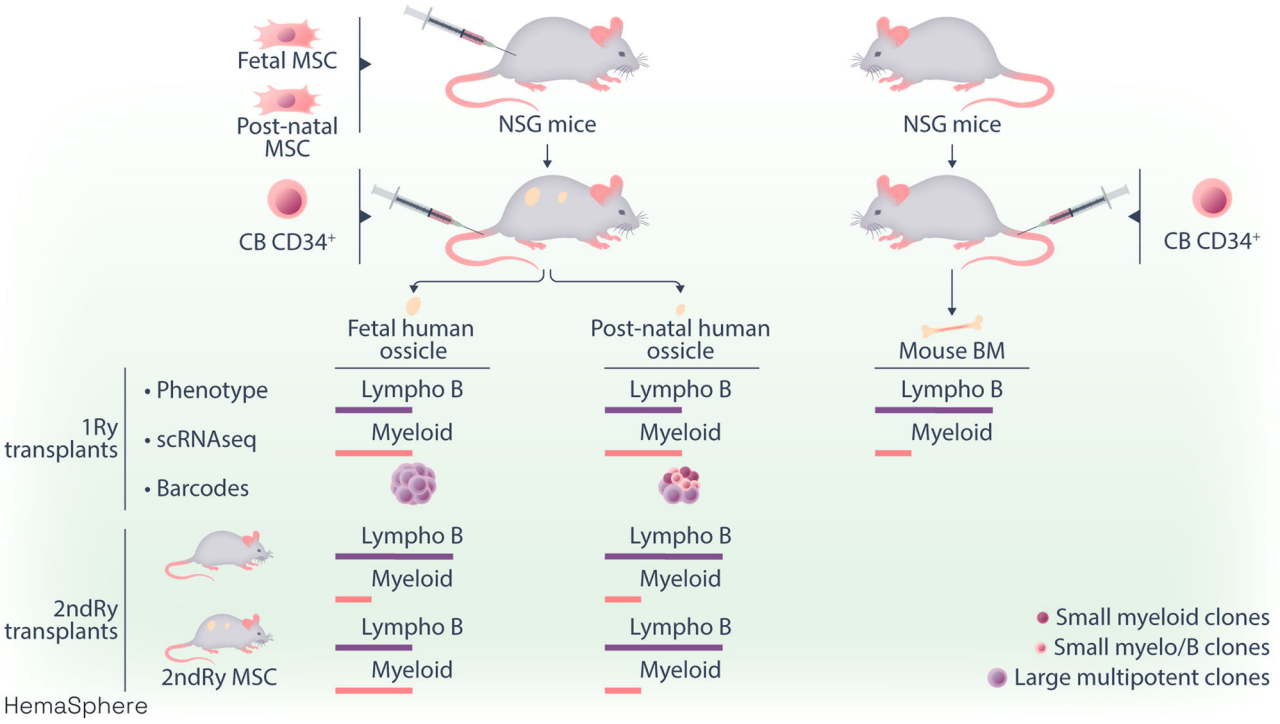

Received: 20 September 2024 | Accepted: 13 February 2025

DOI: 10.1002/hem3.70120

ARTICLE

HemaSphere eha

Orchestration of human multi-lineage hematopoietic cell development by humanized in vivo bone marrow models

Laurent Renou[1,2,3] | Wenjie Sun[4,^] | Chloe Friedrich[5,^] | Klaudia Galant[1,2,3] | Cecile Conrad[4] | Anne Consalus[1,2,3] | Evelia Plantier[1,2,3] | Katharina Schallmoser[6] | Linda Krisch[6] | Vilma Barroca[1,3,7] | Saryami Devanand[1,3,7] | Nathalie Dechamps[1,3,8] | Andreas Reinisch[9,10] | Jelena Martinovic[11] | Alessandra Magnani[12] | Lionel Faivre[13] | Daniel Lewandowski[1,2,3] | Julien Calvo[1,2,3] | Leila Perie[4,^] | Olivier Kosmider[2,5,^] | Françoise Pflumio[1,2,3]

Correspondence: Laurent Renou (laurent.renou@cea.fr); Françoise Pflumio (francoise.pflumio@cea.fr)

Abstract

Hematopoiesis develops in the bone marrow (BM) where multiple interactions regulate the differentiation and preservation of hematopoietic stem and progenitor cells (HSPCs). Immune-deficient murine models have enabled the analysis of molecular and cellular regulation of human HSPCs, but the physiology of these models is questioned as human hematopoietic cells develop in xenogenic microenvironments. In this study, we thoroughly characterized a humanized (h) in vivo BM model, developed from fetal (F/) and post-natal (P-N/) mesenchymal stromal cell (MSC) differentiation (called hOssicles [hOss]), in which human hematopoietic cells are generated following the transplantation of $CD34^+$ cells. Serial isolation and transplant experiments of hMSCs and HSPCs from hOss revealed the dynamic nature of these hBM niches. hOss modified human hematopoietic development by modulating myeloid/lymphoid cell production and HSPC levels, with no major transcriptional changes in HSPCs at the single-cell level. Clonal tracking using genetic barcodes highlighted hematopoietic cell cross-talks between the endogenous murine BM and hOss and differences in clonal myeloid/multipotent cell production between F/hOss and P-N/hOss, uncovering ontogeny-related impact of the BM on human hematopoietic cell production.

INTRODUCTION

Post-natal hematopoiesis takes place in the bone marrow (BM), where numerous cell interactions promote the production of mature blood cells. The analysis of the BM microenvironment in murine models has enabled the detailed characterization of spatially distinct niches of the various types of hematopoietic stem and progenitor cells (HSPCs), including dormant/quiescent and activated hematopoietic stem cells (HSCs).[1–3] Furthermore, single-cell RNA sequence analysis of BM niches has recently revealed the heterogeneous nature of non-hematopoietic cells that support hematopoietic cell production.[4–6]

[1]Université Paris Cité, Inserm, CEA, Stabilité Génétique Cellules Souches et Radiations, LSHL/iRCM/IBFJ, Fontenay-aux-Roses, France
[2]OPALE Carnot Institute, The Organization for Partnerships in Leukemia, Paris, France
[3]Université Paris-Saclay, Inserm, CEA, Stabilité Génétique Cellules Souches et Radiations, LSHL/iRCM/IBFJ, Fontenay-aux-Roses, France
[4]Institut Curie, Université PSL, Sorbonne Université, CNRS UMR168, Laboratoire Physico Chimie Curie, Paris, France
[5]Institut Cochin, CNRS UMR8104, INSERM U1016, Université Paris Cité, Paris, France
[6]Department for Transfusion Medicine and GMP Unit, Paracelsus Medical University, Salzburg, Austria
[7]Animal Experimentation Platform, IRCM, CEA, Fontenay-aux-Roses, France
[8]Flow Cytometry Platform, IRCM, CEA, Fontenay-aux-Roses, France
[9]Department of Internal Medicine, Division of Hematology, Medical University of Graz, Graz, Austria
[10]Department of Blood Group Serology and Transfusion Medicine, Medical University of Graz, Graz, Austria
[11]Fetal Pathology Unit, AP-HP, Hôpital Antoine Beclère, Clamart, France
[12]Biotherapy Department, Hôpital Necker-Enfants Malades, Paris, France
[13]Cell Therapy Unit, AP-HP, Saint Louis Hospital, Paris, France
^Wenjie Sun, Chloe Friedrich, Leila Perie, and Olivier Kosmider co-authors.

Studying the human BM microenvironment is more complicated than murine BM (mBM) as it involves the analysis of BM biopsy sections, which enables only general characterization but not genetic modification of the different cell components, thus greatly limiting the investigation of cell function. Humanized (h)BM models, which are generated ex vivo and in vivo by transplanting human BM cell components into immune-deficient mice, serve as valuable tools in biomedical research.[7,8] These models are designed to replicate the complex cellular interactions that occur in the human BM microenvironment. By recapitulating the physiological conditions, these models provide researchers with a powerful platform to study hematopoiesis, immune cell development, and disease progression. hBM models incorporate components critical for hematopoiesis, such as stromal cells, and extracellular matrix components.[9–14] Inclusion of human endothelial cells that contribute to blood vessel development and are key supportive cells of hematopoiesis in the BM[15,16] has been successfully described in vivo.[9,12,17] Although hBM models are chimeric with murine and human cell components, these systems enable the study of normal and pathological conditions, including hematological disorders, leukemia, and immunodeficiency. Furthermore, these models, which are based on mesenchymal stromal/stem cells (MSCs) and hematopoietic cell differentiation, offer the opportunity to study the effects of various factors, such as infection, therapeutic interventions and response, and genetic mutations that can be incorporated into HSCs or progenitors using CRISPR-Cas9 editing. By providing a controlled and reproducible system, the application of hBM models has proven valuable in cancer research, enabling the analysis of tumor progression, including infiltration and metastasis, in the context of a physiologically relevant microenvironment.[18–20] By providing a platform to evaluate the efficacy and toxicity of anti-cancer drugs, hBM models also facilitate the development of personalized treatment strategies.

It has been hypothesized that species-specific HSC microenvironment interactions are likely vital for human hematopoietic development.[21] However, the impact of humanized niches on human hematopoietic cell recovery generated following $CD34^+$ HSPC transplant has not been assessed.[7] In this study, we aimed to thoroughly characterize a robust and reproducible human ossicles (hOss) hBM model adapted from previous studies.[14] We generated hOss by using human fetal (F) and post-natal (P-N) BM-derived MSCs transplanted subcutaneously into immune-deficient mice. We found that F/hOss and P-N/hOss reproducibly supported human hematopoietic cell development following peripheral injection of human $CD34^+$ umbilical cord blood (CB) cells. Using flow cytometry and single-cell RNA sequencing, characterization of mature and immature human hematopoietic cells developing in hOss revealed a myeloid cell bias at the expense of B lymphoid cells, contrary to that observed in the BM of gold standard NOD scid gamma (NSG) mouse models,[22,23] thus more accurately recapitulating human BM cells. Importantly, recovered hOss contained hMSCs capable of secondary hOss formation and human hematopoietic support, indicating that hOss are dynamic BM structures that maintain functional MSCs. Furthermore, hOss better supported immature human cells capable of higher hematopoietic reconstitution after secondary transplant. Finally, using a cellular barcoding tracking strategy, we found that many human hematopoietic cell clones generated in mice harboring hOss are shared by hOss and mBM, thus indicating important cross-talks between mouse and humanized BM sites. The dynamic hOss structure created a favorable environment for human myelopoiesis and multipotent HSPCs. Differences of myeloid clone sizes between F/hOss and P-N/hOss and the decreased myeloid support in secondary P-N/hOss revealed an ontogeny-related impact on hematopoietic development.

MATERIALS AND METHODS

Human samples

Umbilical CB samples were collected from healthy infants with the informed written consent of the mothers based on the declaration of Helsinki. Samples were obtained in collaboration with Clinique des Noriets, Vitry-sur-Seine, and the Cell Therapy Department in Hôpital Saint Louis, Paris, France. Human BM used in Figure 2E–J were collected from allografts (mostly children sibling donors) at the Cell Therapy Department in Hôpital Saint Louis, Paris, France. Samplings and experiments were acknowledged by the Institutional Review Board of INSERM (Opinion number 13-105-1, IRB00003888). CB and BM cells were subjected to Ficoll gradient. CB mononucleated cells were enriched for $CD34^+$ cells using the human CD34 MicroBeads Kit following manufacturer instructions (130-046-703, Miltenyi Biotec), assessed for purity (≥70% $CD34^+$ cells), and used directly in experiments or froze in fetal bovine serum (FBS, F9665, Sigma-Aldrich) supplemented with 10% DMSO (D5879, Sigma-Aldrich) for later usage. hBM cells were processed for flow cytometry directly after Ficoll.

Fetal bone marrow (F/BM) samples to 12 weeks post-conception were obtained after abortion processes with the informed written consent of the parents in accordance to guidelines approved by the French Agence de Biomédecine (PFS18-009). Samples were obtained in collaboration with the department of Foeto-anatomo-pathology of the Hospital Antoine Beclère, Clamart, France.

Post-natal BM (P-N/BM) MSC samples were collected from healthy children and adult allografts at Necker Enfants Malades hospital, France.

Human MSC (hMSC) isolation and culture

Human F/BM samples were crushed in DPBS with 1% of penicillin–streptomycin (PS). Following centrifugation, the BM fragments were resuspended in α-MEM medium (M4526, Sigma-Aldrich) containing 0.22 µm filtered 10% human platelet lysate provided by the Department for Transfusion Medicine, Paracelsus Medical University, Salzburg, Austria or purchased from StemCell™ Technologies (Stem Cells Lysate, 06962), 1% PS and glutamine, 2 units/mL heparin (hereafter called MSC medium) and incubated in plastic dishes. P-N/BM cells were extracted from filters, centrifuged, and directly plated in MSC medium without Ficoll process. After amplification, adherent cells were split for further expansion (passage 0) or directly plated for experiments.

Mice

All experimental procedures were done in accordance with the recommendations of the European Community (2010/63/UE) and French Ministry of Agriculture regulations (animal facility registration number: A9203202) for the care and use of laboratory animals. Experimental procedures on animal were approved by the French National Animal Care and Use Committee (project A21_021, extension of project A17_009, APAFIS#9458-2017033110277117). NOD.Cg-PrkdcscidIl2rgtm1Wjl/SzJ (NSG), originally purchased from the Jackson Laboratory (Bar Harbor, Maine, USA), were housed and bred in specific pathogen-free animal facilities (Commissariat à l'Energie Atomique et aux Energies Alternatives [CEA], Fontenay-aux-roses, France). Experiments were performed in 8–12-week-old NSG females. At dedicated time points, NSG mice were sublethally irradiated at 2 Gy using a GSRD1-irradiator (137 CS source, GSM,

dose rate 0.97 Gy/min, irradiation plateform of Institut de Radiobiology Cellulaire et Moléculaire, Fontenay-aux-Roses) 4 h before intravenous retro-orbital injection of human CB $CD34^+$ cells under isoflurane anesthesia.

The hOss

The hOss formation protocol was adapted from previous works.[24]

Human hematopoietic development in NSG mice

Two to 8 weeks after hOss implantation, 1×10^5–1×10^6 CB $CD34^+$ cells (100 µL DPBS) were injected intravenously (IV) in the sublethally irradiated mice to generate human hematopoiesis in vivo. Three-months later, mice were sacrificed; two tibiae and two femurs (four long bones, called mBM) and hOss were harvested from euthanized animals; and hematopoietic cells were isolated by flushing the mBM with DPBS and by gently crushing hOss. The isolated cells were maintained on ice during the analysis. Immunophenotyping of human cells was performed using flow cytometry (see later). Counting was realized with a Guava Easycyte 8HT with Muse Count & Viability Kit. Serial transplantation was carried out after flow cytometry measurement of the percent of $hCD34^+$ cells and the counting of total BM/hOss cells, by intravenous injection of $3–5 \times 10^5$ $hCD45^+CD34^+$ cells, recovered from primary recipient mice, in secondary sublethally irradiated animals.

Flow cytometry phenotyping of human/murine hematopoietic cells

The 1×10^6 cells from mBM and hOss were centrifuged, resuspended in 100 µL DPBS, and incubated with antibodies (1/100, all from BioLegend®, otherwise indicated) directed against human CD19 (HIB19), CD14 (61D3), CD15 (W6D3), CD34 (581), CD90 (5E10, BD Biosciences), CD38 (HB-7), and CD45 (HI30) and mouse TER119 (TER-119, 1/500, eBioscience) and mouse CD45 (30-F11, 1/500, BD Pharmingen). Zombie Aqua™ dye was used as a live/dead cell marker (dilution 1/500). All data were acquired on BD FACSCanto™ II and BD LSR II SORP machines with the DIVA software. Compensation controls were performed with single-stained compensation beads. After acquisition, live cells were gated and antibody-labeling analyzed using FlowLogic 7 software.

Statistical analysis

Statistical analysis was performed using GraphPad Prism version 10 software and R software. Values are presented as the median with 95% of confidence interval (CI) or mean ± SEM. Statistical comparisons between conditions were determined using Kruskal-Wallis without correction or Mann–Whitney *U* test or *t-test*. Differences with $p < 0.05$ (*), $p < 0.01$ (**), $p < 0.001$ (***), and $p < 0.0001$ (****) were considered statistically significant.

RESULTS

Development of hOss originating from human BM-derived fetal and post-natal hMSCs

hOss formation was carried out according to a previously developed protocol.[24] Briefly, we first isolated primary hMSCs from F/BM and P-N/BM after cell adhesion on plastic plates. hMSCs were amplified till confluency and split; a portion of the cells were stored frozen at passage 0, while the remaining cells were further amplified for <4 passages for downstream analyses in accordance with the protocol by Passaro et al.[17] Kinetic analysis of cell growth indicated enhanced expansion of the majority (4 of 5) F/hMSCs compared with P-N/hMSCs, reaching statistical significance at day 7 of follow-up only (Figure 1A), mostly dependent on donor difference. Flow cytometry analysis of conventional hMSC markers, such as CD90, CD73, CD105, and CD44, and pan-hematopoietic CD45 and myeloid CD14/CD15 markers and endothelial CD31 confirmed the non-hematopoietic mesenchymal origin of the isolated adherent cells of F/BM and P-N/BM origin (Figure 1B and Supporting Information S3: Figure S1A). No major phenotypic differences were observed between F/hMSCs and P-N/hMSCs. These hMSCs were capable of ex vivo multilineage differentiation into adipogenic, osteogenic, and chondrogenic cells upon exposure to the appropriate cell culture media (Supporting Information S3: Figure S1B). To test the ability to generate hOss, a mixture of hMSCs, cold-matrigel, human platelet lysate, and hBMP-7 was subcutaneously injected into immune-deficient NSG mice that were treated 5 days per week for 4 weeks with parathyroid hormone (to enhance hOss formation and growth) (Figure 1C).[18,24] OsteoSense labeling and tomography analysis, which typically indicates regions with high bone turnover, showed bone remodeling in hOss derived from F/hMSCs and P-N/hMSCs (Supporting Information S3: Figure S1C).[18,25] At 8 weeks post-hMSC implantation, hOss were recovered from grafted mice and analyzed. The F/hMSC-derived hOss were larger and 5 times heavier (median: 579 mg) than P-N/hMSC-derived hOss (median: 94 mg) (Figure 1D,E). Mouse hematopoietic $Ter119^+$ and $CD45^+$ (myeloid $CD11b^+/Gr1^{+/-}$) cells were detected in F/hOss and P-N/hOss, albeit at slightly lower levels compared with mBM, thus showing that murine blood cells perfused the implanted hBM (Figure 1F,G). Histological analysis of hOss sections indicated the presence of active bone structures, including adipocytes and hematopoietic lodges, resembling BM (Figure 1H). Immuno-labeling with anti-mouse endomucin or anti-mouse Meca32 antibodies also revealed vascular networks (Supporting Information S3: Figure S1D,E), thereby confirming that murine blood vessels vascularized hOss. Overall, these results show efficient in vivo development of vascularized BM structures derived from human F/hMSCs and P-N/hMSCs.

Human hematopoiesis in hOss after transplantation of human HSPCs

We next analyzed the human hematopoietic supportive ability of F/hOss and P-N/hOss following intravenous transplantation of human $CD34^+$ cells (10^5 cells/mouse) in sublethally irradiated mice harboring hOss 12 weeks later (Figure 2A).[26] First, we found that the size and weight differences persisted at 12 weeks between F/hOss (median: 390 mg) and P-N/hOss (median: 78 mg) (Supporting Information S3: Figure S2A) as observed in non-transplanted hOss (Figure 1E). Immuno-histochemistry labeling indicated high levels of $hCD45^+$ cells in hOss, comprising $MPO^+/CD14^+$ granulo-monocytic cells, $CD61^+$ megakaryocytes, glycophorin C^+ erythroid cells, and immature $CD34^+$ HSPCs in F/hOss (Figure 2B). Qualitative and quantitative flow cytometry analysis further confirmed human multi-lineage hematopoietic formation in both F/hOss and P-N/hOss at 12 weeks HSPC post-transplant (Figure 2C–J). Erythroid cells were enhanced in F/hOss (10%) and to a lesser extent (albeit not significant) in P-N/hOss (6%) compared to mBM (2%) (Figure 2D), whereas $hCD45^+$ cell percentages were similar in mBM from mice without and with hOss (thus

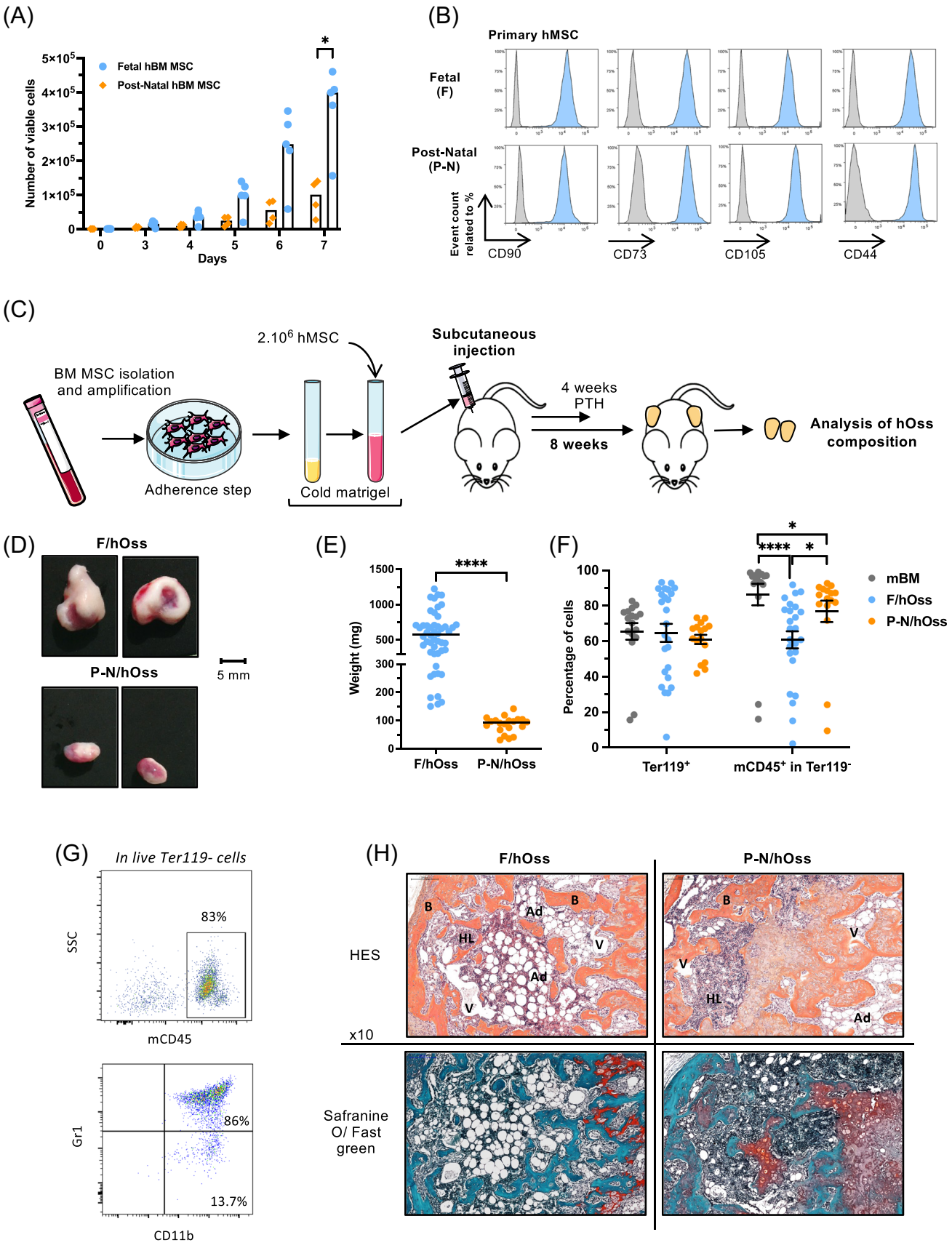

FIGURE 1 (See caption on next page).

FIGURE 1 **Human (h)MSCs from fetal and post-natal bone marrow (BM) generates hOss. (A)** Kinetic of growth of hMSCs isolated from fetal (five hMSCs, age <12 post-conception weeks [PCWs], passage 2) and post-natal BM (four hMSCs, ages: 5, 9, 24, and 51 years, passage 2). Each culture was carried out in quadruplicate. The mean number of cells for each time point for all MSCs is indicated; the median growth of fetal (blue) and post-natal (orange) MSCs are indicated as histograms for each time point. *$p \leq 0.05$; Mann–Whitney *U* test. **(B)** Phenotype of adherent fetal (F28 sample, 11.6 PCWs, passage 2) and post-natal (P-N, ALLO3 sample, 5 years old, passage 2) BM cells. Cells were gated on hCD45$^-$CD14$^-$CD15$^-$CD31$^-$ cells (>90%). Representative of >5 tested hMSC samples. The results were obtained from the gating strategy shown in Supporting Information S3: Figure S1A. **(C)** Experimental protocol of hOss generation using immune-deficient NSG mice. **(D)** Representative pictures of hOss generated from fetal (F/hOss, F28, 11.6 PCWs, passage 1) and post-natal (P-N/hOss, ALLO2, 9 years old, passage 1) hMSCs. hOss were recovered 8 weeks after implantation in mice. **(E)** Weight comparison of F/hOss and P-N/hOss. The results are from nine independent experiments, 11 hMSC samples; 50 hOss (F/hOss) and four independent experiments, five hMSC samples; 20 hOss (P-N/hOss). Each dot represents one hOss. Mean ± SEM are shown in black. ****$p < 0.0001$; Mann–Whitney *U* test. **(F)** Flow cytometry analysis of mouse red blood Ter119$^+$ and total hematopoietic (Ter119$^-$/mCD45$^+$) cells in hOss. Gating was done on FSC/SSC and viable cells. Results were from four independent experiments and eight hMSC samples; 25 hOss (F/hOss) and three independent experiments, four hMSC samples; 16 hOss (P-N/hOss). Mean ± SEM are shown in black. *$p < 0.05$; ****$p < 0.0001$; Kruskal–Wallis test without correction. **(G)** FACS analysis of mouse myeloid CD45$^+$Ter119$^-$ live cells from F/hOss. Results from F17 MSC sample are shown. Representative of 7 F/hOss made out of four fetal MSC lines. **(H)** Representative sample sections with histological staining using HES (upper panels) and Safranin O/Fast Green (lower panels). Ad, adipocytes; B, bone; HL, hematopoietic lodge; V, vessel. Amplification x10.

treated/black signs or not/gray signs with PTH), regardless of the F/or P-N/hMSCs origin (Figure 2E). In terms of absolute numbers, a median of 2.8×10^6 and 3×10^6 hCD45$^+$ cells/hOss were recovered from F/hOss and P-N/hOss, respectively (Supporting Information S3: Figure S2B). The most striking difference was the decreased percentage in CD19$^+$ B cells in F/hOss and P-N/hOss (46% and 53% of hCD45$^+$ cells, respectively) compared to mBM from mice without hOss, in which B cells predominated (80%) ($p \leq 0.01$, Figure 2F) as typically observed in these humanized mouse models.[23] Inversely, myeloid cell levels (CD14$^+$/CD15$^+$) were higher in hOss (34% and 27%) compared to mBM (10%) ($p \leq 0.001$, Figure 2G). Only a discrete difference was measured in B/myeloid/erythroid cell levels between F/hOss or P-N/hOss. Comparing B/myeloid/erythroid cell levels between mBM from mice with and without hOss showed a similar, albeit less pronounced, decrease in B cell ($p \leq 0.01$) and an increase in myeloid cells ($p \leq 0.001$) in mBM from mice with hOss (Supporting Information S3: Figure S2E–H), thus highlighting possible cross-talks between hOss and mBM sites. Analysis of immature human cell compartments indicated similar levels of CD34$^+$ HSPCs among hCD45$^+$Lin$^-$ cells in F/hOss, P-N/hOss, and mBM without hOss at 12 weeks post-injection of CD34$^+$ cells (Figure 2H). Assessing more immature hCD45$^+$Lin$^-$CD34$^+$CD38$^-$ HSPCs showed also similar levels in F/hOss and in P-N/hOss, whereas higher hCD45$^+$Lin$^-$CD34$^+$CD38$^-$CD90$^+$ HSC were detected in F/hOss and in P-N/hOss (Figure 2I,J). Compared with mBM witho ut hOss, CD34$^+$Lin$^-$ cells were significantly increased in mBM with F/hOss and mBM with P-N/hOss, while no difference was observed in hCD45$^+$Lin$^-$CD34$^+$CD38$^-$/CD90$^+$ HSCs (Supporting Information S3: Figure S2I–K). These results show that hOss enable human hematopoiesis development, and differences were detected primarily in phenotypically mature hematopoietic cells compared to mBM, but also in immature HSC, independently of hMSC samples used (different symbols, Figure 2D–J). Interestingly, most levels of B cells, myeloid cells, and immature cells in hOss fell between mBM and hBM from young healthy donors (median age: 11 years) (black squares, Figure 2E–J), thereby suggesting that hOss enhance the support of the mouse models to normal human hematopoiesis.

Fetal and post-natal hOss contain functional human mesenchymal stem cells

To characterize the possible replenishment of hOss by engrafted resident hMSCs, we tested whether isolation of hMSCs from primary hOss was possible and whether these recovered hMSCs could generate secondary hOss. After crushing primary F/hOss or P-N/hOss, adherent cells were recovered and amplified in plastic plates (Figure 3A). Flow cytometry analysis of adherent cells (using antibodies specific for the same hMSC markers as displayed in Figure 1B) confirmed that the cells were human mesenchymal cells (Figure 3B). The secondary isolated hMSCs were injected into mouse flanks to form hOss, and human CD34$^+$ cells (10^5 cells/mouse) were transplanted 8 weeks later (Figure 3A). Upon sacrifice of the mice at 12 weeks post-transplant, secondary hOss had successfully formed; interestingly, these secondary F/hOss were twice as large (mg) as secondary P-N/hOss (Figure 3C,D), albeit this difference was slightly less pronounced than that observed in primary hOss (Figure 1E and Supporting Information S3: Figure S2B). Murine erythroid and hematopoietic cells were present in secondary hOss that did not receive CD34$^+$ umbilical CB cells, although lower levels were observed compared to mBM (Figure 3E). Human erythroid cells were enhanced in secondary F/hOss, as observed in primary hOss, but not in P-N/hOss (Figure 3F). The percentage of human hematopoietic cells did not vary between mBM and secondary F/hOss, but were significantly higher in secondary P-N/hOss compared to mBM (Figure 3G), in relation with its respective low erythroid cell level. In terms of absolute number of hCD45$^+$ cells, a significant decrease was observed in secondary P-N/hOss compared with F/hOss (Supporting Information S3: Figure S3A) and this result ought to be cautiously considered as only one P-N/hOss was used to generate six hOss. Compared to mBM from mice without hOss, secondary F/hOss displayed a significant decrease in CD19$^+$ B cells and a significant increase in CD14$^+$/CD15$^+$ myeloid/GPA$^+$ erythroid cells, while this difference was not observed in secondary P-N/hOss (Figure 3H,I). Analysis of immature cells revealed similar percentage of hCD34$^+$Lin$^-$/CD38$^-$ HSPC between F/and P-N/hOss, while increased percentage of hCD34$^+$CD90$^+$ HSC was detected only in secondary F/hOss compared to mBM, confirmed at the absolute cell number levels (Figure 3J–M). As analyzed in mice with primary hOss, mBM from mice with secondary hOss mostly displayed similar human hematopoietic reconstitution to that observed in secondary hOss, again outlining possible cross-talks between mBM and hOss (Figure 3F–L). Comparison between hematopoietic cells from primary and secondary hOss further confirmed subtle but significant differences between F/hOss and P-N/hOss. Indeed, F/hOss appeared to effectively support balanced production of human lymphoid and myelo-erythroid cells, whereas secondary P-N/hOss displayed reduced development of human myelo-erythroid cells (Supporting Information S3: Figure S3B–E). Besides, percentage of immature HSPC (hCD34$^+$/Lin$^-$ and hCD34$^+$/CD38$^-$) compartments were mostly similar between primary and secondary hOss with differences being observed in hCD34$^+$/CD90$^+$ cells between F/and P-N/hOss, the latter exhibiting lowest levels (Supporting Information S3: Figure S3F,H). Overall, these results show that hOss are dynamic human BM-like structures

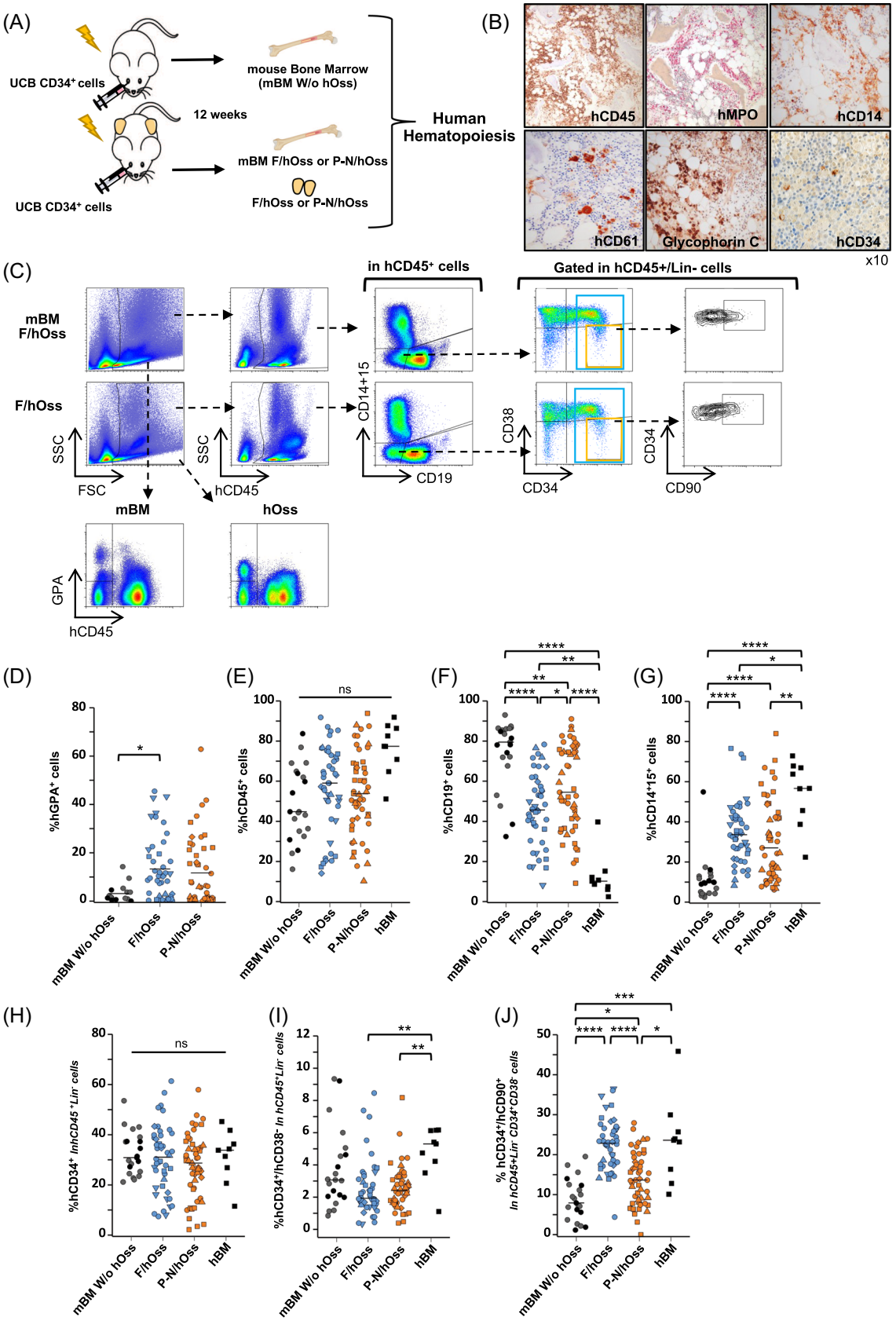

FIGURE 2 (See caption on next page).

FIGURE 2 **Human fetal hOss and post-natal hOss support normal human hematopoiesis. (A)** Experimental design of xenografts of umbilical cord blood (UCB) $CD34^+$ cells in mice with or without hOss. **(B)** Immuno-histology labeling of sections of F/hOss injected with UCB $CD34^+$ and analyzed at 12 weeks with human hematopoietic cells (hCD45), myeloid cells (hMPO, CD14), megakaryocytes (CD61), red cells (Glycophorin C), and immature HSPCs (CD34). Amplification, x10. **(C)** Representative flow cytometry analysis of the human hematopoietic cells developing in mBM (upper panel) and F/hOss (lower panel) recovered from the same mouse 12 weeks post-injection of UCB $CD34^+$ cells. Dashed arrows indicate the sequential gating strategies. **(D)** Percentage of human GPA^+ cells in hOss and mBM of mice without hOss. Gating as in **(C)**. Each dot represents individual mice (mBM without hOss: $n = 21$ mice, black and gray signs from two independent experiments: respectively treated and not treated with PTH; F/hOss: $n = 25$ mice, 47 hOss from five different hMSC samples (F28, circle; F37, square; F35, diamond; F1, rectangle; F18, inverted rectangle); P-N/hOss: $n = 28$ mice, 51 hOss obtained from four different hMSCs (ALLO3, circle; ALLO4: square; ALLO5, diamond; ALLO2, rectangle). Black line shows the median value. **(E)** Percentage of cells expressing $hCD45^+$ gated as in C for mBM and hOss 12 weeks post-transplant of UCB $CD34^+$ cells. Same mice and same hMSC as in **(D)**. Black line shows the median value. **(F, G)** Percentage of human lymphoid $CD19^+$ B cells **(F)** and myeloid $CD14^+/CD15^+$ cells **(G)**. Cells were gated in $hCD45^+$ as in **(C)**. hBM cells from healthy donors (age <18 years, $n = 9$) are included. Same mice and same hMSC as in **(D)** and **(E)**. The gating strategy is depicted in Supporting Information S3: Figures S2D and S2C. **(H–J)** Percentage of $CD34^+$ **(H)** and $CD34^+CD38^-$ HSPCs **(I)** gated in $hCD45^+Lin^-(CD19^-CD14^-CD15^-)$ cells as in **(C)** and of $hCD34^+CD90^+$ HSC (J) gated in $hCD45^+Lin^-CD34^+CD38^-$ cells. hBM cells from healthy donors (age <18 years, $n = 9$) are included. Same mice and same hMSC as in **(D)** and **(E)**. Black line shows the median value. $^*p < 0.05$; $^{**}p < 0.01$; $^{***}p < 0.001$; $^{****}p < 0.0001$; Kruskal–Wallis test without correction. ns, no statistical difference.

that contain hMSCs capable of serial production of hOss that continue to support human hematopoietic development. Interestingly, the lympho-myeloid bias observed in primary P-N/hOss was no longer observed in secondary P-N/hOss, thus suggesting that skewed lineage commitment may occur during the transplant process.

Immature human hematopoietic cells from hOss display enhanced HSC functional potential

We next characterized the immature cell function of hOss-engrafted $CD34^+$ HSPCs using standard assays, such as myelo/erythroid colony forming units (CFUs) to measure committed progenitor levels and secondary reconstitution of immune-deficient mice to detect HSCs.[27] Cells were obtained from primary hOss and the BM of mice with and without hOss as controls. Human $CD34^+$ HSPCs were quantified and either plated in semi-solid methylcellulose medium or transplanted into NSG mice (Figure 4A). Assessing colonies (i.e., progenitors) did not reveal major differences in numbers and composition between hOss and mBM (Figure 4B,C and Supporting Information S3: Figure S4). On the contrary, increased reconstitution potential of human HSPCs recovered from primary hOss was detected compared with mBM from mice without hOss (Figure 4D,E). Mice injected with cells from mBM with hOss also displayed $hCD45^+$ cells, which levels were also greater than in mice injected with cells from mBM without hOss, similar to mice receiving cells from hOss (Figure 4E). The human hematopoietic cells recovered from secondary NSG mice were primarily composed of B lymphoid cells, regardless of origin (hOss and mBM) (Figure 4F). Strong secondary engraftment of $hCD45^+$ cells with high B and low myeloid cell percents was also detected in mice injected with cells from secondary hOss-bearing mice (Supporting Information S3: Figure S4B–D). Together, these results show that hOss maintain a stronger human HSC potential than mBM of mice without hOss. Interestingly, the enhanced myeloid cell differentiation observed in hOss (Figures 2 and 3) was lost in the mBM of secondary NSG mice in the absence of the hOss environment.

Gene expression profiles reveal enhanced myeloid and decreased lymphoid precursors/progenitors in $hCD34^+$ cells from fetal and post-natal hOss

To further characterize the immature cell compartment engrafting hOss compared to mBM from mice without hOss, we performed single-cell RNA sequencing of $hCD34^+$ cells sorted at 12 weeks post-transplant (Figure 5A). A total of 9894 cells, containing 3188, 4005, and 2701 cells from mBM without hOss, F/hOss, and P-N/hOss, respectively, were successfully integrated in UMAP (Supporting Information S3: Figure S5A,B). Seurat unsupervised clustering (resolution levels = 0.2) was applied to separate cells into 13 clusters according to the gene expression profile.[28] Comparing these results with the expression profiles described in Hay et al.,[29] the 13 clusters were classified according to cell differentiation pathway, which highlighted lymphoid ($CD34^+$ Multilin/CLP, $CD34^+$ pre-B cycling, $CD34^+$ pro-B cycling, $CD34^+$ pre-plasma cell [Pre-PC]), myeloid (immature neutrophils/monocytes, neutrophils), erythroid, and dendritic cell populations ($CD34^+$ early erythroblasts, erythroblasts, $CD34^+$ MDP/pre-dendritic and dendritic) (Figure 5B,C). Cell cluster annotation revealed that 70.5% of cells (6975 cells) were either B-cell lineage oriented ($CD34^+$ pre-PC and pre-B cell cycling) or multilineage HSCs/progenitors ($CD34^+$ Multilin/CLP and $CD34^+$ HSC/MPP/LMPP) (Figure 5D). The other immature cells (immature neutrophils/monocytes, $CD34^+$ MDP/pre-dendritic cells, $CD34^+$ Eo-B-Mast, $CD34^+$ early erythroblasts, erythroblasts) were detected at lower levels. The repartition of these cell subpopulations/clusters indicated variations among cells isolated from hOss and mBM; for example, early erythroblasts and neutrophils (clusters 7 and 9) were frequent in P-N/hOss cells, while $CD34^+$ eosinophils-basophiles-mastocytes (cluster 8) were highly represented in F/hOss (Supporting Information S3: Figure S5C). When progenitors/precursors were grouped into B lymphoid (including $CD34^+$ pre-PC, $CD34^+$ pre-B cycling, $CD34^+$ Multilin/CLP, $CD34^+$ pro-B, $CD34^+$ pre-B, follicular B cells), myeloid/erythroid (immature neutrophils/monocytes, neutrophils, $CD34^+$ MDP/pre-dendritic cells, $CD34^+$ Eo-B-Mast, $CD34^+$ early erythroblasts, erythroblasts), and early HSPC ($CD34^+$HSC/MPP/LMPP) lineages, significant differences were observed between mBM and hOss (Figure 5E) that were similar to variations observed in the mature cell compartments (Figure 2E–J). Indeed, this analysis showed that immature cells from F/hOss and P-N/hOss comprise significantly reduced B lymphoid precursors/progenitors ($p < 0.0001$, χ^2 test) and increased myeloid/erythroid precursors/progenitors (F/hOss vs. mBM, $p < 0.0001$; P-N/hOss vs. mBM, $p < 0.0001$, χ^2 test) compared to mBM from mice without hOss. We also observed a slightly enhanced proportion of HSC/MPP/LMPP cells in hOss (Figure 5E,F/hOss vs. mBM, $p < 0.0001$, P-N/hOss vs. mBM, $p = 0.0015$, χ^2 test), in accordance with the results of the functional assays displayed in Figure 4D–F.

We also assessed whether hOss could impact gene expression in the most immature $CD34^+$ HSC/MPP/LMPP cells of our data set. We analyzed the most differentially expressed genes in the HSC/MPP/LMPP cell cluster isolated from hOss and mBM. Comparing P-N/hOss

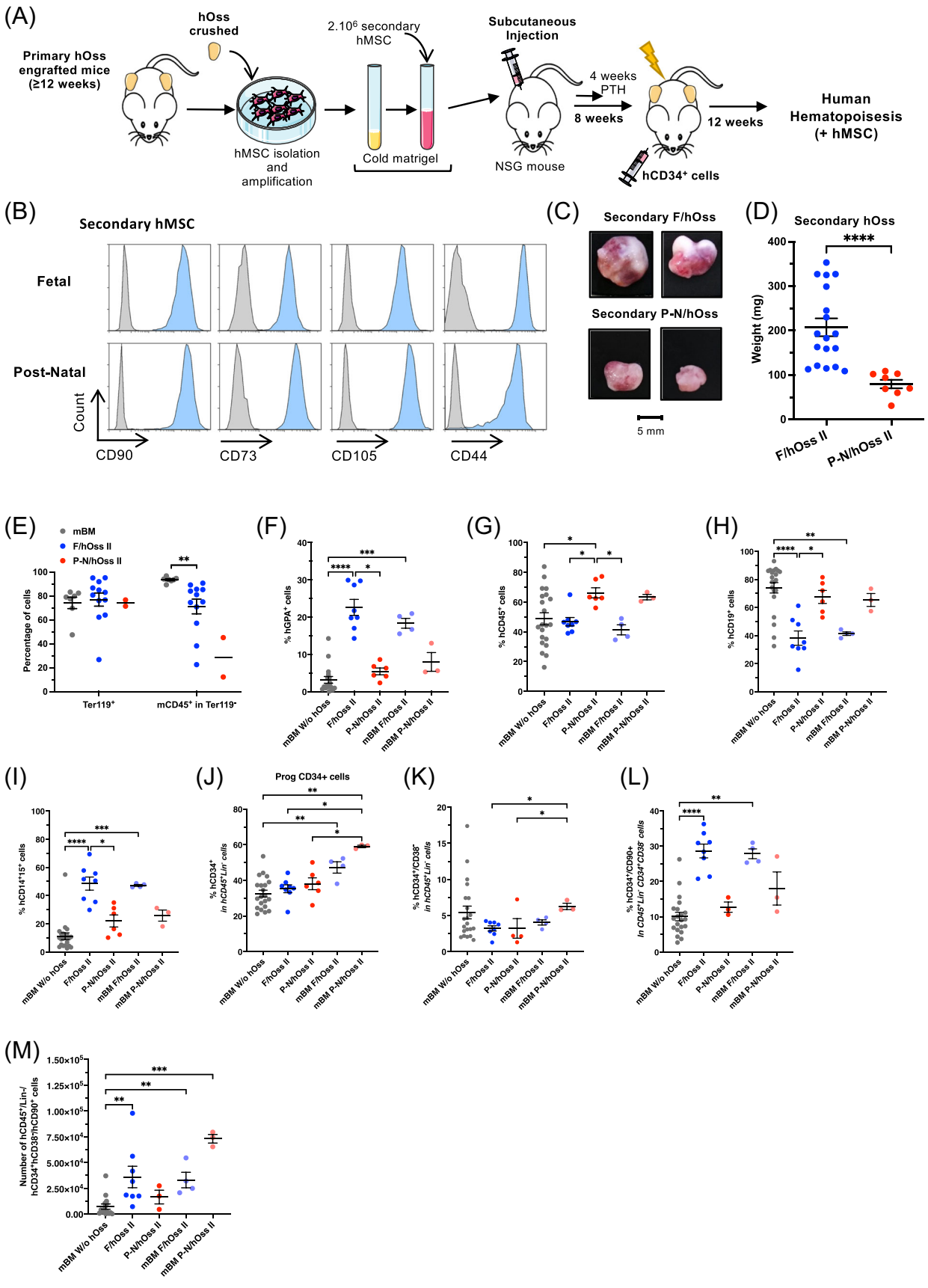

FIGURE 3 (See caption on next page).

FIGURE 3 **Human primary hOss comprises hMSCs capable of secondary hOss development. (A)** Experimental design of secondary (II) hOss formation and grafts of UCB CD34$^+$ cells in mice carrying secondary hOss. Secondary hMSCs were isolated from hOss implanted ≥12 weeks before with primary hMSC. **(B)** Flow cytometry analysis of secondary hMSCs isolated from primary F/and P-N/hOss. Gating on hCD45$^-$CD14$^-$CD15$^-$CD31$^-$ cells (>90%) as in Supporting Information S3: Figure S1A. Representative of >4 tested secondary hMSC samples. **(C)** Representative secondary hOss obtained 10–12 weeks post-injection of secondary hMSCs. Results from hMSC samples F28 (11.6 PCWs) and ALLO3 (5 years old). **(D)** Weight comparison of secondary (II) F/hOss and P-N/hOss. Results from 18 hOss (two starting F/hMSCs, three independent experiments) and eight hOss (one P-N/hMSCs, two independent experiments). Shown in black are mean ± SEM. **(E)** Percentage of murine cells analyzed by flow cytometry, recovered from secondary hOss from mice without injection of umbilical cord blood CD34$^+$ cells. Gating as in Figure 1. The results are from 12 hOss (one secondary F/hMSC in two independent experiments) and two hOss (one secondary P-N/hMSC in one experiment). Black line shows the median value. **(F)** Percentage of human GPA$^+$ cells in mBM from mice with and without secondary (II) hOss. Gating strategy as in Figure 2C. Shown are individual values of mBM from 21 mice without hOss (gray dots: same mice/values displayed in Figure 2D), eight hOss generated by two secondary F/hMSCs in four mice (dark blue dots), six hOss generated by one secondary P-N/hMSC in three mice (dark red dots), six mBM from mice with secondary F/hOss (light blue dots) and three mBM from the mice with secondary P-N/hOss (pale red dots). Black line shows the median value. **(F)** Percentage of GPA$^+$ cells in secondary hOss at 12 weeks post-transplant of UCB CD34$^+$ cells. **(G)** Percentage of hCD45$^+$ cells. Same mice as in **(F)**. Gating as shown in Figure 2C. **(H, I)** Percentage of human lymphoid B cells (CD19$^+$) **(H)** and myeloid cells (CD14$^+$/CD15$^+$) **(I)** gated in hCD45$^+$ cells according to gating in Figure 2C. Same mice as in **(F)** and **(G)**. Black line shows the median value. **(J–L)** Percentage of CD34$^+$ **(J)** and CD34$^+$CD38$^-$ HSPCs **(K)** gated in hCD45$^+$Lin$^-$ (CD19$^-$CD14$^-$CD15$^-$) cells, and CD34$^+$CD90$^+$ HSC (**L**) gated in hCD45$^+$Lin$^-$ CD34$^+$CD38$^-$ cells, with the gating strategy as in Figure 2C. Same mice as in **(F)** and **(G)**. (**M**) Number of CD34$^+$CD90$^+$ HSC cells gated in hCD45$^+$Lin$^-$CD34$^+$CD38$^-$ in hOss described in (**L**) Black line shows the median value. $^*p < 0.05$; $^{**}p < 0.01$; $^{***}p < 0.001$; $^{****}p < 0.0001$. **(D)** Mann–Whitney *U* test. **(F–M)** Kruskal–Wallis test without correction.

and mBM, we identified 318 differentially expressed genes ($p < 0.05$), of which 298 genes were upregulated and 20 genes were downregulated in P-N/hOss-derived cells (Figure 5F). Comparing F/hOss and mBM, we found 4443 differential genes (1130 upregulated genes and 3313 downregulated genes in F/hOss) (Figure 5G). The 50 most upregulated genes are presented in Supporting Information S2: Tables S1 and S2. Examination of the two lists of upregulated genes revealed 47 common genes, of which nine genes were included among the 50 most upregulated genes in both F/hOss and P-N/hOss (Figure 5H,I and Supporting Information S2: Tables S1–S3). Among these nine genes, *LRRC75A* (Leucin-rich Repeat Containing 75A protein) has recently been implicated in the regulation of VEGF in ischemic BM-MSC, and VEGF is a regulator of HSC function.[30] However, *VEGF* was not enhanced in our HSC/MPP/LMPP data set, thus suggesting that *LRRC75A* enhancement does not impact *VEGF* transcriptional levels in immature cells, in accordance with the finding that VEGF is typically produced by endothelial cells. To further examine the modified processes in hOss-derived cells, we performed KEGG and GO enrichment analyses using the 100 most deregulated genes in P-N/hOss and F/hOss compared to mBM. We found that metabolic pathways/OXPHOS-cell respiration was enriched in P-N/hOss, and several pathways unrelated to HSC function/potential were slightly enriched in F/hOss (Supporting Information S3: Figure S5D). We also assessed several other gene sets more specific to hematopoietic cells (listed in Supporting Information S2: Table S4) but did not observe enrichment in any specific pathway, including in stemness, in HSC/MPP/LMPP cells from hOss compared to mBM. Overall, these results revealed only a discreet qualitative distinction between the HSC compartments recovered from hOss and mBM. However, we observed a slightly increased proportion of HSCs in hOss and a bias toward B lymphoid/myelo-erythroid differentiation at the progenitor/precursor levels, which may contribute to the observed mature cell variations and the enhanced functional HSC.

Clonal tracking shows that hOss promote the human myelopoietic cell lineage in both hOss and the mBM of mice with hOss

We next used lentiviral barcoding to label and track CD34$^+$ HSPC-driven hematopoietic reconstitution at the clonal level in hOss and mBM (Figure 6A). CD34$^+$ cells from umbilical CB were transduced with 21-bp lentiviral barcode libraries containing 40×10^4 different barcodes expressing GFP.[31] Low transduction efficiency was used (7.8%–16.8% GFP$^+$ cells, Supporting Information S3: Figure S6A and Supporting Information S2: Table S5) to ensure that most cells were labeled with one barcode. Transduced cells were injected into mice with or without hOss and hematopoietic GFP$^+$ CD19$^+$ B cells, CD14$^+$CD15$^+$ myeloid cells, and CD34$^+$ immature cells were sorted from hOss and mBM at 12 weeks after injection (Figure 6A, Supporting Information S3: Figure S6B). At that time point, GFP$^+$ and GFP$^-$ HSPCs had generated the same proportion of each cell lineage fraction (Supporting Information S3: Figure S6C), thus showing very limited differentiation bias from the transduced and non-transduced cells. After filtering and quality control (Supporting Information S3: Figure S6D), we obtained variable barcode numbers between mice, which was neither correlated with the presence of hOss nor the hOss origin (Supporting Information S2: Table S5). Based on the number of injected CD34$^+$ umbilical CB cells and the transduction efficiency, we estimated the frequency of HSCs at 1/1000 to 1/100 (Supporting Information S2: Table S5), which is in accordance with a previous study using barcoded human HSCs.[32] We then assessed hematopoietic variations between mice with and without hOss. In the mBM without hOss, the progeny of barcoded HSPCs was primarily biased toward B cells (left triangle plot, Figure 6C), whereas in mice with hOss, the barcoded HSPCs more uniformly yielded B cells and myeloid cells (middle and right triangle plots, Figure 6C), which is in agreement with flow cytometry results shown in Figure 2. In mice bearing hOss, we found an increased proportion of clones containing myeloid cells, which was statistically significant for mice with P-N/hOss (Supporting Information S3: Figure S6E). No difference was observed in total barcodes (Figure 6B) or the number of cells produced per barcode (clone size) when hOss and mBM of mice with hOss were compared with mBM without hOss, with the exception of myeloid clones in the P-N/hOss condition, which were significantly smaller (Supporting Information S3: Figure S6F). Thus, the increased myeloid to B lymphoid ratio observed at the population level in P-N/hOss was associated with an increase in small myeloid-biased clones and not to an increased production of total myeloid cells per clone. We next used the barcodes to investigate the relationship between human hematopoiesis developed in hOss and mBM in the same mice. More than 40% of clones/barcodes were common between the hOss and mBM (Supporting Information S3: Figure S6G and in Figure 6D,E), thus indicating that many hematopoietic cells originating from the same HSPC were distributed in both sites. These observations provided insights into the mechanisms of phenotypic similarities between mBM from mice with hOss and hOss-containing cells at the population level (Supporting Information S3: Figure S2C–H). The

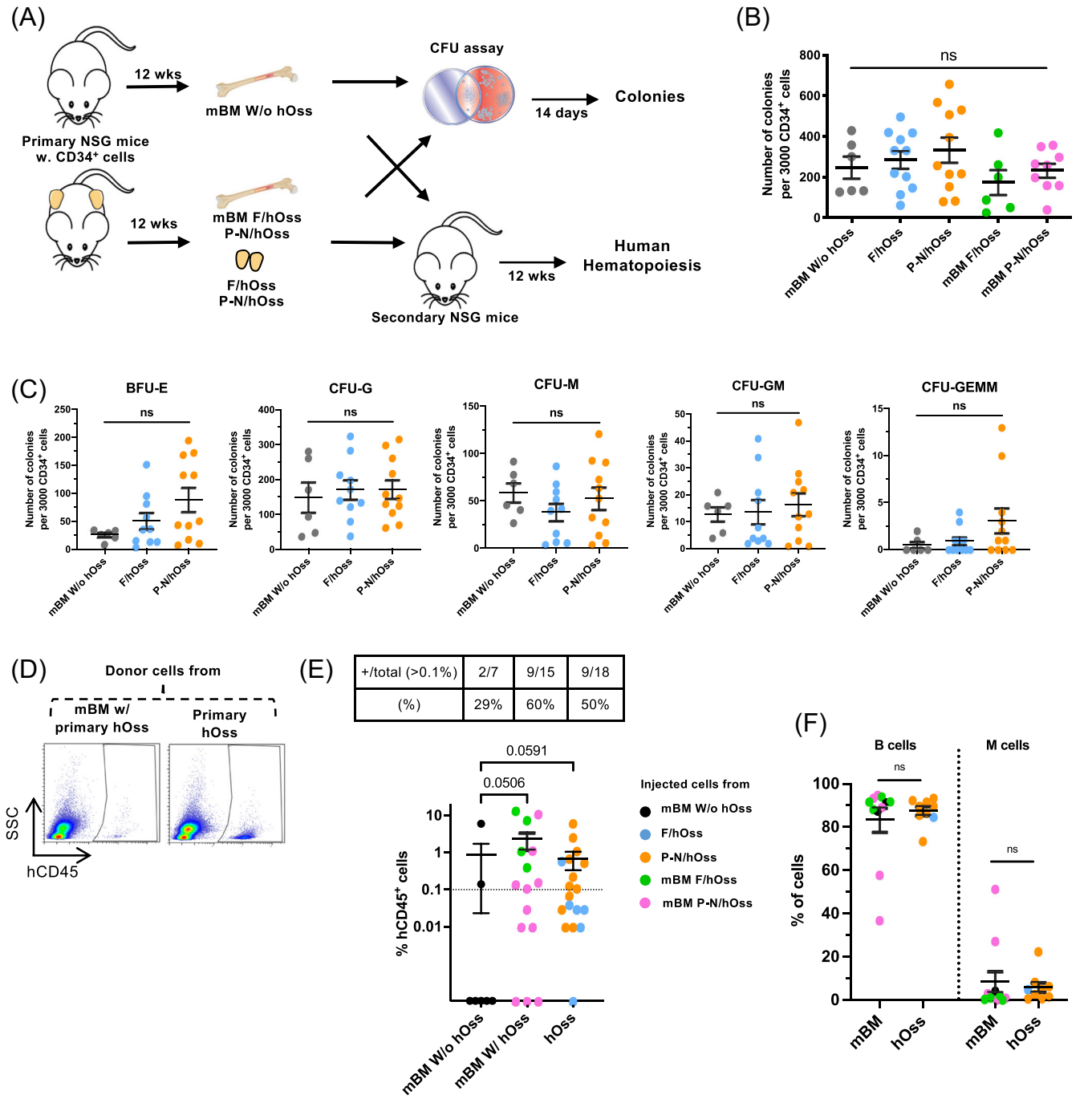

FIGURE 4 **Human primary hOss display enhanced levels of functional immature human cells. (A)** Experimental design of the functional analysis of the immature cell compartment in primary hOss compared with murine bone marrow (mBM) from mice with and without hOss. $CD34^+$ cells recovered from crushed hOss and mBM were analyzed by flow cytometry, plated in methylcellulose semi-solid medium (1×10^3 $hCD34^+$ cells/plate), or injected into secondary NSG mice ($3–5 \times 10^5$ $hCD34^+$ cells/mouse). **(B)** Total numbers of colonies generated by 3000 plated $CD34^+$ cells isolated from different BM sites (mBM without hOss, gray dots; F/hOss, blue dots; P-N/hOss, orange dots; mBM with F/hOss, green dots; mBM with P-N/hOss, pink dots). Results are from three independent experiments. Shown in black are mean ± SEM. ns, not significant; Kruskal–Wallis test without correction. **(C)** Total number of granulocytic (CFU-G), monocytic (CFU-M), granulo-monocytic (CFU-GM), erythroid (BFU-E), or multipotent (CFU-GEMM) colonies generated by 3000 plated $CD34^+$ cells. Black lines indicate the median values. ns, not significant; Kruskal–Wallis test without correction. **(D)** Representative FACS plots of $hCD45^+$ cells detected in the mBM of NSG mice injected with cells from mBM of mice with hOss and from hOss (both primary sites). Gated on FSC/SSC parameters. **(E)** Upper panel: ratio of secondary mice engrafted with >0.1% of $hCD45^+$ cells per total injected mice and associated percentage. Lower panel: percentage of $hCD45^+$ cells in the BM of NSG mice injected with cells from mBM mice without (seven mice) and with primary hOss (15 mice) and from primary hOss (18 mice). Shown in black are mean ± SEM. ns, not significant; Kruskal–Wallis test without correction. **(F)** Relative percentage of lymphoid B ($CD19^+$) and myeloid ($CD14^+$/$CD15^+$) cells from the mice in **(E)**. Only mice with ≥0.1% $hCD45^+$ cells are included. Shown in black are mean ± SEM; Kurskal–Wallis test.

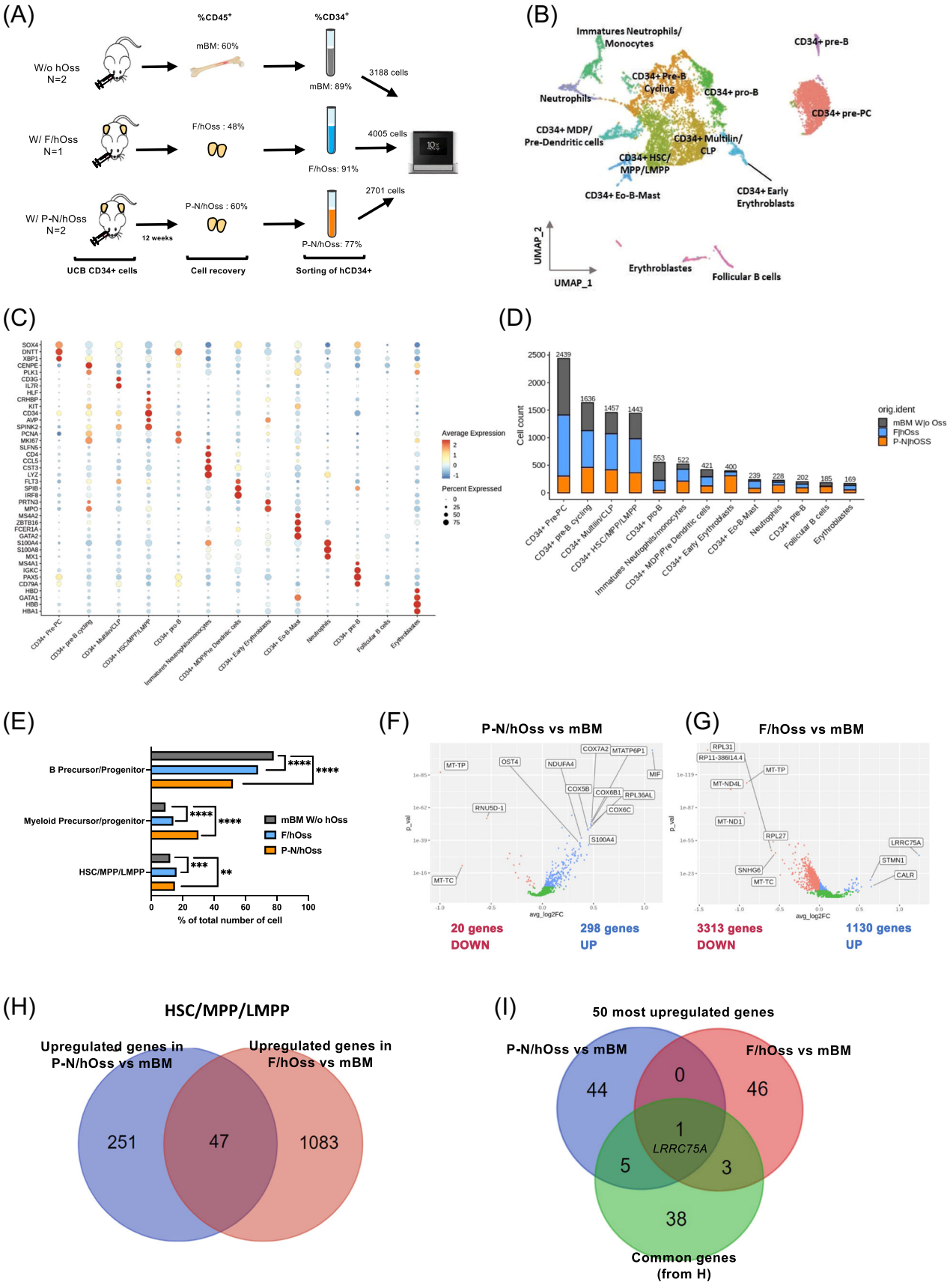

FIGURE 5 (See caption on next page).

FIGURE 5 **Single-cell analysis of immature cells recovered from hOss: enhanced bias toward myelo/erythroid progenitors and increased HSC levels. (A)** Experimental design. Three months after injection of 10^5 UCB $CD34^+$ cells, mononuclear cells were isolated from mBM and hOSS and pooled according to origin. $CD34^+$ cells were sorted with a purity >70% and viability >90% and processed for single-cell RNA-sequencing libraries. **(B)** UMAP representation of the 13 clusters identified via Seurat. Each cluster is represented by a different color. Clusters were annotated by comparing the gene expression profiles with those of the hematopoietic populations described by Hay et al.[6,27] HSC, hematopoietic stem cell; MPP, multipotent progenitor; LMPP, lymphoid-primed multi-potential progenitor; MDP, monocyte/dendritic cell progenitor; CLP, common lymphoid progenitor; Multi-Lin, multi-lineage progenitor; pre-PC, pre-plasma cells; Eo-B-Mast, eosino-baso-mast cells. **(C)** Annotation of the 13 clusters according to gene markers as described.[6,27] Color code in the figure legend. **(D)** Comparison of population distribution (in absolute numbers) between mBM and hOss compartments. Each bar corresponds to the total number of cells in a given subpopulation. The sum of each bar corresponds to the total number of cells in our data set. Each bar is divided into three segments corresponding to the original samples. **(E)** Comparison of the proportion of progenitor groups (HSC/MPP/LMPP, B-cell precursors/progenitors, and myeloid precursor/progenitor cells) in mBM and hOss. Proportions were calculated within each sample using the data from **(D)**. "B Precursor/Progenitor" include $CD34^+$ pre-PC, $CD34^+$ pre-B cycling, $CD34^+$ Multilin/CLP, $CD34^+$ pro-B, $CD34^+$ pre-B, follicular B cells. "Myeloid precursor/progenitor" contains immature neutrophils/monocytes, neutrophils, $CD34^+$ MDP/pre-dendritic cells, $CD34^+$ Eo-B-Mast, $CD34^+$ early erythroblasts, erythroblasts. Early HSPC are contained in $CD34^+$HSC/MPP/LMPP cells. The proportions were compared using a χ^2 test with $^{**}p < 0.01$, $^{***}p < 0.001$, $^{****}p < 0.001$. **(F, G)** Differentially expressed genes between post-natal hOss **(F)** or fetal hOss **(G)** and mBM cells within the $CD34^+$ HSC/MPP/LMPP compartment. Each volcano plot indicates the expression of genes that were significantly downregulated ($p < 0.05$, red) or upregulated (blue) in hOss compared to mBM. Genes that were not significantly underexpressed or overexpressed are shown in green. **(H)** Venn diagram showing the 47 common upregulated genes in the $CD34^+$ HSC/MPP/LMPP compartment from P-N/hOss (blue) and F/hOss (red), both compared to mBM. **(I)** Venn diagram showing nine out of the 47 gene list (green) from **(H)**, identified among the 50 most upregulated genes of P-N/hOss compared to mBM (blue) and F-hOss compared to mBM (red) lists.

common cells constituted mainly large multipotent clones (pink dots in Figure 6D,E) in which $CD34^+$ immature cells were also detected, which is indicative of self-renewal properties. Clones uniquely present in one BM site were also detected (Supporting Information S3: Figure S6G and red dotted line boxes in Figure 6D,E) and found at similar levels in mBM and F/hOss, whereas more unique clones were detected in P-N/hOss (Supporting Information S3: Figure S6G). Interestingly, while mice with F/hOss were primarily reconstituted with large multipotent clones detected both in mBM and hOss (Figure 6D and Supporting Information S3: Figure S6H), mice with P-N/hOss displayed clones with variable size, and a trend of enhanced myeloid-bearing cell clones that were detected in both mBM and hOss or only in P-N/hOss (Figure 6E and Supporting Information S3: Figure S6I). Overall, our results indicate that a diversity of multipotent or more lineage-restricted HSPC clones reconstitute human hematopoiesis in both the mBM and hOss in these models, many of which were common between BM sites at 12 weeks post-transplant. The presence of hOss creates a more favorable environment for human myelopoiesis in large clones in F/hOss and more variable/small-sized clones in P-N/hOss.

DISCUSSION

In this study (summarized in Supporting Information S3: Figure S7), we show that hBM hOss models support the capacity of human hematopoietic cell differentiation and production. The hOss also exhibit intrinsic self-replenishing potential by maintaining implanted hMSCs capable of serial functional hBM formation and hematopoietic support. These results are concordant with previously described hBM models that display efficient human hematopoietic support following HSPC transplant, including balanced production of mature myeloid cells compared with mature lymphoid cells,[9,12,13,20] thus demonstrating that the results between different hOss models are reproducible. Such a myeloid bias was detected, regardless of whether the MSCs used to form hOss were of fetal or P-N origin. However, P-N/MSC-derived hOss and mBM displayed more-variable/smaller myeloid-biased HSPC clones compared with mice with F/hOss, in which myeloid cells were produced from more multipotent clones. These results suggest that even if the developmental origin of MSCs did not significantly impact hematopoietic cell type recovery at the population level, there are important differences between F/hOss and P-N/hOss niches in terms of the type of clones that reconstitute human hematopoietic cells.

It was previously unknown whether this bias in lineage cell production originated from biased differentiation of HSCs or progenitors toward the myeloid lineage at the expense of the lymphoid lineage. In our study, we questioned this point using gene expression profiles in $CD34^+$ cells isolated from hOss and mBM at the single-cell level. Our results indicate that HSPCs are not properly lineage biased at the transcriptional level, as lineage commitment programs were not different in HSPCs isolated from hOss, compared with mBM. The single-cell RNA sequencing results rather highlighted the presence of larger myeloid and erythroid progenitor/precursor compartments, which is probably supported by human factors produced by the humanized microenvironment of hOss.[9,14,20] These results are in accordance with previous findings from a BM model generated by implanting collagen scaffolds carrying hMSCs, which displayed enhanced myeloid progenitors, as assessed by cell surface marker and CFU-C analysis.[13] However, when secondary transplants were performed in regular NSG mice (without hOss), even though HSC levels were enhanced in both models (our results and Fritsch et al.[13]), we did not observe an increased myeloid bias in human $CD45^+$ cells derived from hOss, thus indicating that without the hOss influence, the myeloid potential of human HSPCs is no longer detected. The enhancement in myeloid production observed in previous studies was probably due to the recipient mouse models used (STRG and MSTRG), which produce human myeloid cytokines.[13] Our results indicate that mice with hOss can substitute cytokine-humanized mice in terms of myeloid cell lineage production from engrafted HSCs.

Indeed, using NSG recipient mice that do not produce human factors, we found that primary hOss had a strong impact on human hematopoiesis, which was detected from mature cells to immature cells, and was observed from hOss to the mBM of mice with hOss. Importantly, and original from previous studies, the hOss impact on lineage properties persisted in MSCs isolated from primary hOss, as observed in human hematopoietic cells recovered from secondary hOss, especially when hOss formation was of fetal origin, thus suggesting that Fetal MSCs are more potent than post-natal MSC in generating equilibrated lympho-myeloid lineages at the long term in those models. These results further indicate that hOss are dynamic multicellular structures that maintain MSCs with the ability to differentiate in hOss capable of perpetuating cell lineage in a balanced manner, which is an established feature of BM. Interestingly, in one study in which hOss were implanted after HSPCs had engrafted mBM, the balanced myeloid-lymphoid progeny was observed in hOss.[33] This finding is in line with our results of mBM from hOss-bearing mice, thus displaying the impact of hOss both in proximity

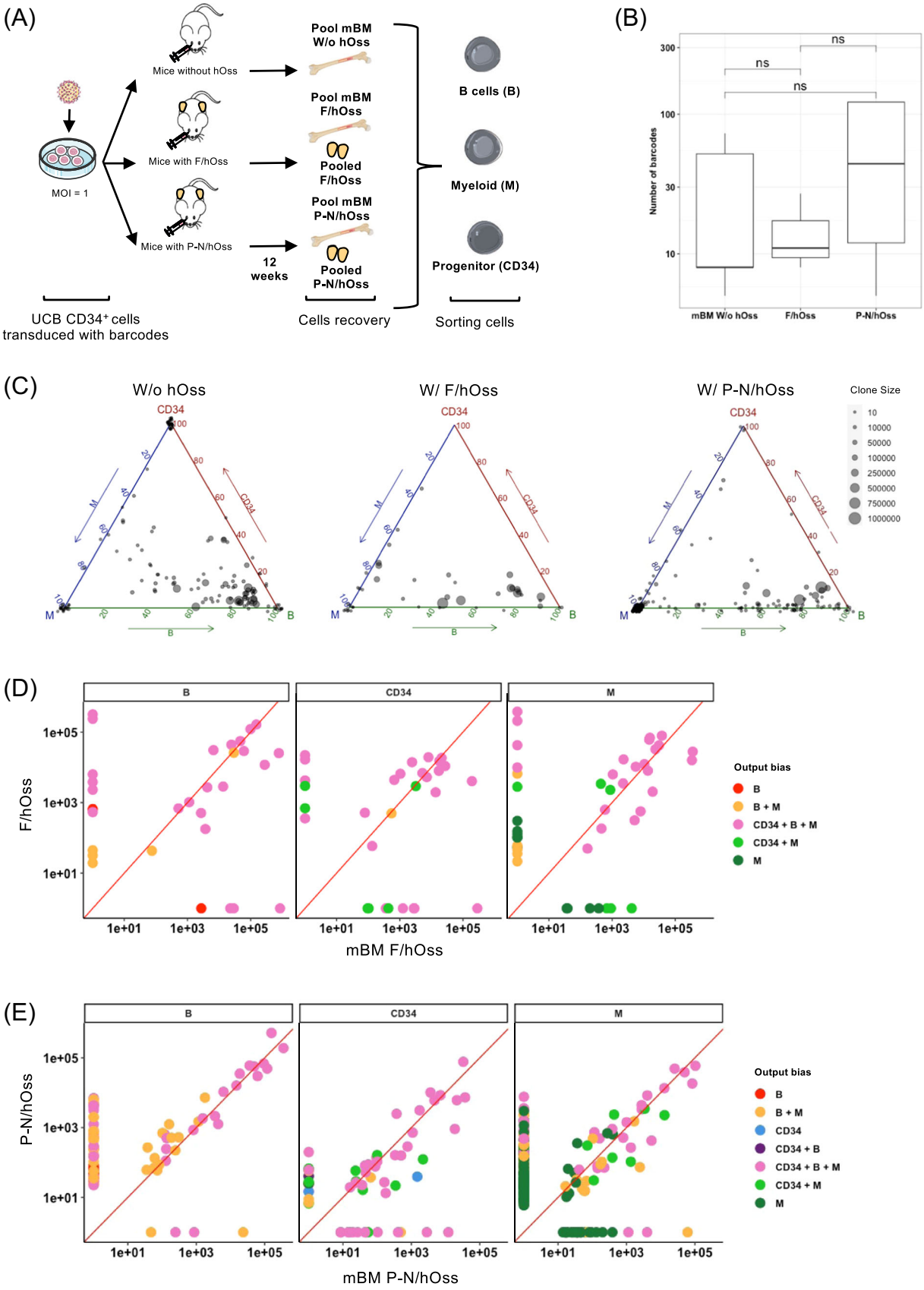

FIGURE 6 (See caption on next page).

FIGURE 6 **Cellular barcoding shows that hOss support more balanced human hematopoietic development**. **(A)** Experimental design: Injection of 10^5 UBC $CD34^+$ cells after barcode transduction. Three months later, mononucleated cells were isolated from mBM and hOss. Transduced (GFP^+) B, myeloid (M), and $CD34^+$ cells were sorted, lyzed, and barcodes were amplified by PCR for identification and analysis. **(B)** The number of unique barcodes identified per mouse in each condition. ns, not significant; *t*-test. **(C)** Ternary plot of the fraction of cells produced per barcode clone in each of the three cell types ($CD34^+$, lymphoid B cells, and myeloid [M] cells). Each dot represents a distinct barcode. The size of the dot indicates the number of cells originating from each injected barcoded progenitor (clone size). The number of reads per barcode clones detected in the hOss and BM for F/hOss **(D)** and P-N/hOss **(E)** in the various cell types. Each dot represents a distinct barcode. The axis is $\log_{10}$ transformed of the renormalized read count +1. The threshold for lineage content is 1%, and the minimal clone size is 10 cells.

and at a distance. Using clonal tracking of hematopoietic cell production, we show that in hOss-grafted mice, many human hematopoietic cells recovered from mBM and hOss originated from multipotent HSPCs common between mBM and hOss, especially in F/hOss. Such clones were also detected independently in hOss or mBM, although they were rarer, thus highlighting that at 12 weeks post-transplant, human hematopoiesis in such models occurs through differentiation of multipotential HSCs. Furthermore, smaller unipotent myeloid cell clones were present in hOss, especially in P-N/hOss, potentially associated with different waves of progenitor differentiation or concomitant production of hematopoietic cells by a diversity of HSPCs, as previously described.[32] The extent to which hOss and mBM compete to attract HSCs versus committed progenitors remains to be assessed using kinetic analyses. Also, whether the common clonally related hematopoietic cells are due to exchanges of differentiated cells between mBM and hOss or are rather generated from single barcoded HSCs that divided, trafficked through the blood stream and settled in the mBM and hOss to differentiate remains to be examined.

In this study, we also investigated whether the developmental age of BM from which MSCs were recovered impacted hOss formation and hematopoietic support. Previous studies on human F/MSCs, pediatric MSCs and adult MSCs have reported variations in cell surface marker expression and fibroblast CFUs, outlining specificities in F/MSCs.[34] In mice, several age-related BM microenvironment factors modulate HSC potency, including osteopontin, which enhances levels in young adults compared with older adults -attenuating aging of old HSCs, and the CCL5/RANTES, which is a secreted matrix protein that contributes to the bias in old HSCs toward myeloid differentiation.[35,36] In our experiments, both F/MSC and P-N/MSC reproducibly formed hOss, with increased size and weight in F/MSC-derived hOss, which was likely associated with higher bone density. Such differences did not dramatically impact hematopoietic cell production at the population level, at least in primary hOss, with a trend toward myeloid progenitors only detected by single-cell RNA-seq in P-N/MSC-derived hOss compared with F/MSC-derived hOss. Interestingly, secondary hOss perpetuated the variations in size albeit to a lesser extent, and P-N/hOss lost the myeloid-lymphoid lineage balance, indicative of exhaustion most likely mediated by stress-induced serial transplantation. Further research is necessary to understand the drift mechanisms in primary MSCs undergoing hOss formation. The possible aging caveat of serial tissue culture-isolated MSCs and the difficulty to reproduce hOss formation from one lab to the next has recently been challenged.[37] A human telomerase-immortalized mesenchymal cell line, Mesenchymal Sword of Damocles, has been shown to recapitulate the various multipotent and hematopoietic supportive properties of primary hMSCs by generating hOss in vivo after ex vivo priming to chondrocyte or osteocyte differentiation.[20] Such a cell line is a valuable tool as it produces >1000 hOss originating from a clonal cell population.[20] hOss obtained from Mesenchymal Sword of Damocles cells and primary MSC samples are also useful recipients of pathologic cells, such as acute myeloblastic leukemia and BM-infiltrating solid tumor cells (breast cancer and neuroblastoma). This approach enables analysis of the relationship between the BM microenvironment and pathologic cells in a humanized context, including the soluble factors involved.[10,12,14,18,20,38]

These results contribute novel findings regarding the distinct impact of hBM models generated from hMSCs isolated from normal fetal and post-natal donors on normal hematopoietic development after transplantation of human HSPCs. Continued advancements in these models, such as the incorporation of human endothelial cell-derived vasculature,[17] will undoubtedly further impact normal and abnormal hematopoietic cell development. However, detailed characterization at the clonal levels, as described here, is essential to validate the physiological relevance of these models to study normal and abnormal human blood cells.

ACKNOWLEDGMENTS

We acknowledge the help of B. Burroni, from the Hôpital Cochin, Paris, France (immuno-histo-chemistry labeling of hOss sections), and the people from the technical platforms of Institut de Radiobiology Cellulaire et Moléculaire, IBFJ/CEA, Fontenay-aux-Roses, France, in particular, V. Ménard from the irradiation platform, D. Busso and G. Piton from the molecular bioengineering platform, J. Baijer and A. Schmitz from the flow cytometry platform, S. Messian from IRCM, J. Rivière and M. Vilotte from INRAE for hOss sections and histochemistry. We are grateful to F. Duconge who helped with tomography, and C. Antoniewski and L. Bellenger from ARTbio Bioinformatics Analysis Facility from Sorbonne University. We acknowledge the Fetopathology Department of Antoine Béclère Hospital, Clamart, France; The Clinique des Noriets, Vitry-sur-Seine, France; and the Cell Therapy Department from Hôpital Saint Louis, Paris, France, for providing human CB and BM samples. We thank the patients for agreeing to help scientific research. We thank S. Teinrera Bento for help with barcode PCR in the troubleshooting phase of the project and F. Cayrac from the BMBC facility for the barcode lentivirus production. We thank E. Solary, N. Drouin, and C. Jego (Gustave Roussy, Villejuif, France) and C. Dussiau (Institut Cochin, Paris) who participated in the early days of the project. S. Moore edited the manuscript for English language.

AUTHOR CONTRIBUTIONS

Laurent Renou, Chloe Friedrich, Klaudia Galant, Cecile Conrad, Evelia Plantier, Vilma Barroca, Saryami Devanand, Daniel Lewandowski, and Nathalie Dechamps performed experiments. Laurent Renou, Wenjie Sun, Chloe Friedrich, and Julien Calvo performed scRNAseq and barcoding bioinformatic analyses. Katharina Schallmoser, Linda Krisch, Andreas Reinisch, Jelena Martinovic, Alessandra Magnani, and Lionel Faivre provided extremely important materials. Leila Perie, Olivier Kosmider, and Françoise Pflumio supervised the work. Laurent Renou, Chloe Friedrich, Wenjie Sun, and Julien Calvo created the figures. Laurent Renou and Françoise Pflumio wrote the manuscript. All authors read and approved the manuscript content.

CONFLICT OF INTEREST STATEMENT

The authors declare no conflict of interest.

DATA AVAILABILITY STATEMENT

The data that support the findings of this study are openly available in GEO at https://www.ncbi.nlm.nih.gov/geo/query/acc.cgi?acc=GSE263857 (reference number GSE263857).

FUNDING

This work received institutional grants from INSERM, CEA, Université Paris Saclay, and Université Paris Cité. The study was also supported by ITMO-Cancer (3R Program, édition 2020 and MIC Program, édition 2022), CONECT-AML Pair-Pédiatrie program, Ligue Nationale Contre le Cancer (F. P.: équipe labellisée 2021–2023), and the Fondation ARC pour la recherche contre le Cancer (ARC, F. P.: équipe labellisée 2019–2021).

ORCID

Laurent Renou https://orcid.org/0009-0005-7793-8544
Françoise Pflumio http://orcid.org/0000-0001-8995-596X

SUPPORTING INFORMATION

Additional supporting information can be found in the online version of this article.

REFERENCES

1. Ding L, Morrison SJ. Haematopoietic stem cells and early lymphoid progenitors occupy distinct bone marrow niches. *Nature*. 2013;495(7440):231-235. doi:10.1038/nature11885
2. Cordeiro Gomes A, Hara T, Lim VY, et al. Hematopoietic stem cell niches produce lineage-instructive signals to control multipotent progenitor differentiation. *Immunity*. 2016;45(6):1219-1231. doi:10.1016/j.immuni.2016.11.004
3. Pinho S, Marchand T, Yang E, Wei Q, Nerlov C, Frenette PS. Lineage-biased hematopoietic stem cells are regulated by distinct niches. *Dev Cell*. 2018;44(5):634-641.e4. doi:10.1016/j.devcel.2018.01.016
4. Tikhonova AN, Dolgalev I, Hu H, et al. The bone marrow microenvironment at single-cell resolution. *Nature*. 2019;569(7755):222-228. doi:10.1038/s41586-019-1104-8
5. Baryawno N, Przybylski D, Kowalczyk MS, et al. A cellular taxonomy of the bone marrow stroma in homeostasis and leukemia. *Cell*. 2019;177(7):1915-1932.e16. doi:10.1016/j.cell.2019.04.040
6. Baccin C, Al-Sabah J, Velten L, et al. Combined single-cell and spatial transcriptomics reveal the molecular, cellular and spatial bone marrow niche organization. *Nature Cell Biol*. 2020;22(1):38-48. doi:10.1038/s41556-019-0439-6
7. Abarrategi A, Mian SA, Passaro D, Rouault-Pierre K, Grey W, Bonnet D. Modeling the human bone marrow niche in mice: from host bone marrow engraftment to bioengineering approaches. *J Exp Med*. 2018;215(3):729-743. doi:10.1084/jem.20172139
8. Dupard SJ, Grigoryan A, Farhat S, Coutu DL, Bourgine PE. Development of humanized ossicles: bridging the hematopoietic gap. *Trends Mol Med*. 2020;26(6):552-569. doi:10.1016/j.molmed.2020.01.016
9. Chen Y, Jacamo R, Shi Y, et al. Human extramedullary bone marrow in mice: a novel in vivo model of genetically controlled hematopoietic microenvironment. *Blood*. 2012;119(21):4971-4980. doi:10.1182/blood-2011-11-389957
10. Antonelli A, Noort WA, Jaques J, et al. Establishing human leukemia xenograft mouse models by implanting human bone marrow-like scaffold-based niches. *Blood*. 2016;128(25):2949-2959. doi:10.1182/blood-2016-05-719021
11. Groen RWJ, Noort WA, Raymakers RA, et al. Reconstructing the human hematopoietic niche in immunodeficient mice: opportunities for studying primary multiple myeloma. *Blood*. 2012;120(3):e9-e16. doi:10.1182/blood-2012-03-414920
12. Abarrategi A, Foster K, Hamilton A, et al. Versatile humanized niche model enables study of normal and malignant human hematopoiesis. *J Clin Invest*. 2017;127(2):543-548. doi:10.1172/JCI89364
13. Fritsch K, Pigeot S, Feng X, et al. Engineered humanized bone organs maintain human hematopoiesis in vivo. *Exp Hematol*. 2018;61:45-51.e5. doi:10.1016/j.exphem.2018.01.004
14. Reinisch A, Thomas D, Corces MR, et al. A humanized bone marrow ossicle xenotransplantation model enables improved engraftment of healthy and leukemic human hematopoietic cells. *Nat Med*. 2016;22(7):812-821. doi:10.1038/nm.4103
15. Ramasamy SK, Kusumbe AP, Itkin T, Gur-Cohen S, Lapidot T, Adams RH. Regulation of hematopoiesis and osteogenesis by blood vessel-derived signals. *Annu Rev Cell Dev Biol*. 2016;32:649-675. doi:10.1146/annurev-cellbio-111315-124936
16. Itkin T, Gur-Cohen S, Spencer JA, et al. Distinct bone marrow blood vessels differentially regulate haematopoiesis. *Nature*. 2016;532(7599):323-328. doi:10.1038/nature17624
17. Passaro D, Abarrategi A, Foster K, Ariza-McNaughton L, Bonnet D. Bioengineering of humanized bone marrow microenvironments in mouse and their visualization by live imaging. *J Vis Exp*. 2017;126:55914. doi:10.3791/55914
18. Martine LC, Holzapfel BM, McGovern JA, et al. Engineering a humanized bone organ model in mice to study bone metastases. *Nat Protoc*. 2017;12(4):639-663. doi:10.1038/nprot.2017.002
19. Thibaudeau L, Quent VM, Holzapfel BM, Taubenberger AV, Straub M, Hutmacher DW. Mimicking breast cancer-induced bone metastasis in vivo: current transplantation models and advanced humanized strategies. *Cancer Metastasis Rev*. 2014;33(2-3):721-735. doi:10.1007/s10555-014-9499-z
20. Grigoryan A, Zacharaki D, Balhuizen A, et al. Engineering human minibones for the standardized modeling of healthy hematopoiesis, leukemia, and solid tumor metastasis. *Sci Transl Med*. 2022;14(666):eabm6391. doi:10.1126/scitranslmed.abm6391
21. Holzapfel BM, Hutmacher DW, Nowlan B, et al. Tissue engineered humanized bone supports human hematopoiesis in vivo. *Biomaterials*. 2015;61:103-114. doi:10.1016/j.biomaterials.2015.04.057
22. Pflumio F, Izac B, Katz A, Shultz L, Vainchenker W, Coulombel L. Phenotype and function of human hematopoietic cells engrafting immune-deficient CB17-severe combined immunodeficiency mice and nonobese diabetic-severe combined immunodeficiency mice after transplantation of human cord blood mononuclear cells. *Blood*. 1996;88(10):3731-3740.
23. Henry E, Souissi-Sahraoui I, Deynoux M, et al. Human hematopoietic stem/progenitor cells display reactive oxygen species-dependent long-term hematopoietic defects after exposure to low doses of ionizing radiations. *Haematologica*. 2020;105(8):2044-2055. doi:10.3324/haematol.2019.226936
24. Reinisch A, Hernandez DC, Schallmoser K, Majeti R. Generation and use of a humanized bone-marrow-ossicle niche for hematopoietic xenotransplantation into mice. *Nat Protoc*. 2017;12(10):2169-2188. doi:10.1038/nprot.2017.088
25. Lambers FM, Stuker F, Weigt C, et al. Longitudinal in vivo imaging of bone formation and resorption using fluorescence molecular tomography. *Bone*. 2013;52(2):587-595. doi:10.1016/j.bone.2012.11.001
26. Dykstra B, Kent D, Bowie M, et al. Long-term propagation of distinct hematopoietic differentiation programs in vivo. *Cell Stem Cell*. 2007;1(2):218-229. doi:10.1016/j.stem.2007.05.015
27. Robin C, Pflumio F, Vainchenker W, Coulombel L. Identification of lymphomyeloid primitive pogenitor cells in fresh human cord blood and in the marrow of nonobese diabetic–Severe combined immunodeficient (NOD-SCID) mice transplanted with human CD34+

cord blood cells. *J Exp Med*. 1999;189(10):1601-1610. doi:10.1084/jem.189.10.1601

28. Hao Y, Hao S, Andersen-Nissen E, et al. Integrated analysis of multimodal single-cell data. *Cell*. 2021;184(13):3573-3587.e29. doi:10.1016/j.cell.2021.04.048
29. Hay SB, Ferchen K, Chetal K, Grimes HL, Salomonis N. The Human Cell Atlas bone marrow single-cell interactive web portal. *Exp Hematol*. 2018;68:51-61. doi:10.1016/j.exphem.2018.09.004
30. Miura T, Kouno T, Takano M, et al. Single-cell RNA-seq reveals LRRC75A-expressing cell population involved in vegf secretion of multipotent mesenchymal stromal/stem cells under ischemia. *Stem Cells Transl Med*. 2023;12(6):379-390. doi:10.1093/stcltm/szad029
31. Eisele AS, Cosgrove J, Magniez A, et al. Erythropoietin directly remodels the clonal composition of murine hematopoietic multipotent progenitor cells. *eLife*. 2022;11:e66922. doi:10.7554/eLife.66922
32. Cheung AMS, Nguyen LV, Carles A, et al. Analysis of the clonal growth and differentiation dynamics of primitive barcoded human cord blood cells in NSG mice. *Blood*. 2013;122(18):3129-3137. doi:10.1182/blood-2013-06-508432
33. Reinisch A, Etchart N, Thomas D, et al. Epigenetic and in vivo comparison of diverse MSC sources reveals an endochondral signature for human hematopoietic niche formation. *Blood*. 2015;125(2):249-260. doi:10.1182/blood-2014-04-572255
34. Maijenburg MW, Kleijer M, Vermeul K, et al. The composition of the mesenchymal stromal cell compartment in human bone marrow changes during development and aging. *Haematologica*. 2012;97(2):179-183. doi:10.3324/haematol.2011.047753
35. Guidi N, Sacma M, Ständker L, et al. Osteopontin attenuates aging-associated phenotypes of hematopoietic stem cells. *EMBO J*. 2017;36(10):1463. doi:10.15252/embj.201796968
36. Ergen AV, Boles NC, Goodell MA. Rantes/Ccl5 influences hematopoietic stem cell subtypes and causes myeloid skewing. *Blood*. 2012;119(11):2500-2509. doi:10.1182/blood-2011-11-391730
37. Côme C, Balhuizen A, Bonnet D, Porse BT. Myelodysplastic syndrome patient-derived xenografts: from no options to many. *Haematologica*. 2020;105(4):864-869. doi:10.3324/haematol.2019.233320
38. Vaiselbuh SR, Edelman M, Lipton JM, Liu JM. Ectopic human mesenchymal stem cell-coated scaffolds in NOD/SCID mice: an in vivo model of the leukemia niche. *Tissue Eng Part C Methods*. 2010;16(6):1523-1531. doi:10.1089/ten.tec.2010.0179